J. Fluid Mech. (1990), *vol.* 231, *pp.* 113–133
Printed in Great Britain

Throughflow effects on convective instability in superposed fluid and porous layers

By FALIN CHEN
Institute of Applied Mechanics, National Taiwan University, Taipei, Taiwan 10764, ROC

(Received 23 August 1990 and in revised form 12 March 1991)

We implement a linear stability analysis of the convective instability in superposed horizontal fluid and porous layers with throughflow in the vertical direction. It is found that in such a physical configuration both stabilizing and destabilizing factors due to vertical throughflow can be enhanced so that a more precise control of the buoyantly driven instability in either a fluid or a porous layer is possible. For $\zeta = 0.1$ (ζ, the depth ratio, defined as the ratio of the fluid-layer depth to the porous-layer depth), the onset of convection occurs in both fluid and porous layers, the relation between the critical Rayleigh number R_m^c and the throughflow strength γ_m is linear and the Prandtl-number (Pr_m) effect is insignificant. For $\zeta \geqslant 0.2$, the onset of convection is largely confined to the fluid layer, and the relation becomes $R_m^c \sim \gamma_m^2$ for most of the cases considered except for $Pr_m = 0.1$ with large positive γ_m where the relation $R_m^c \sim \gamma_m^3$ holds. The destabilizing mechanisms proposed by Nield (1987*a*, *b*) due to throughflow are confirmed by the numerical results if considered from the viewpoint of the whole system. Nevertheless, from the viewpoint of each single layer, a different explanation can be obtained.

1. Introduction

We consider the effect of throughflow on the convective instability of a combined fluid and porous layer system which is heated from below. The boundaries at the top and bottom are rigid and held at constant temperatures. The throughflow effect on the convective instability in either the fluid or the porous layer has been extensively discussed by several investigators. In the porous layer, these include Wooding (1960), Sutton (1970), Homsy & Sherwood (1976), Jones & Persichetti (1986), and Nield (1987*a*); in the fluid layer, examples are Shvartsblat (1968, 1969, 1971), Krishnamurti (1975), Gershuni & Zhukhovitskii (1976), Somerville & Gal-Chen (1979), and Nield (1987*b*). The throughflow effect in the fluid layer is of interest because of the possibility of controlling the convective instability by adjusting the throughflow. In the porous layer, the *in situ* processing of energy resources such as coal, oil shale, or geothermal energy often involves the throughflow in the porous medium. The importance of buoyancy-driven instability in such systems may become significant when precise processing is required.

The throughflow effect in a porous medium was first considered by Wooding (1960), who treated the case in which the base-state temperature field is dominated by the convective effects on the throughflow. The domain in his analysis is semi-infinite in the vertical direction, in which a large upward throughflow is provided. Later Sutton (1970) presented a linear stability analysis for small throughflow with rigid and conducting boundaries at both top and bottom and insulating walls at the sides. Homsy & Sherwood (1976) extended the analysis of Sutton to larger

throughflow and considered a laterally infinite domain. These investigations all concluded that the throughflow stabilized the convection in the porous layer. In considering the applications in packed beds, such as the reaction zone in a catalytic reactor or an ion exchange column, Jones & Persichetti (1986) studied the stability limits in a porous medium bounded at top and bottom by either impermeable or porous boundaries. On the impermeable (or rigid) boundary the perturbed vertical velocity vanishes while on the porous (or free) boundary the perturbed vertical velocity can be non-zero. They found that a small amount of throughflow can provide a destabilizing effect in at least one situation, when the throughflow is from a rigid boundary towards a free boundary. They stated that the origin of the destabilizing mechanism was not completely understood, although they eliminated numerical error as a possible one.

As pointed out by Homsy & Sherwood (1976) as well as by Gershuni & Zhukhovitskii (1976), however, the effect of throughflow is to confine significant thermal gradients to a thermal boundary layer at the boundary toward which the throughflow is directed. The effective lengthscale is thus smaller than the layer thickness and so the effective Rayleigh number of the porous layer, which is proportional to the lengthscale, is much less than the actual $R_{\mathrm{m}}^{\mathrm{c}}$. A larger value of $R_{\mathrm{m}}^{\mathrm{c}}$ is thus necessary to initiate the convection. The throughflow, therefore, is a stabilizing effect. The cause of the destabilizing effect uncovered by Jones & Persichetti (1986) was not immediately clear until the analytical solution was provided by Nield (1987*a*). He indicated that destabilization occurs when the throughflow is away from the more restrictive boundary (the dynamically rigid boundary) and toward the less restrictive boundary (the dynamically free boundary). The throughflow then decreases the temperature gradient near the restrictive boundary and increases it in the rest of the medium. Consequently, the maximum of perturbed temperature occurs at a place where the perturbed vertical velocity is largest. This leads to an increase in energy supply for destabilization. In that case, the throughflow is destabilizing.

The effect of throughflow in the fluid layer is more complex because the Prandtl number (Pr) comes into play. Being interested in the vertical asymmetry associated with the stability of hexagonal cells, Krishnamurti (1975) and Somerville & Gal-Chen (1979) investigated the effects of small amounts of throughflow. Gershuni & Zhukhovitskii (1976) summarized the results obtained by Shvartsblat (1968, 1969, 1971) and concluded that the effect of throughflow is stabilizing and is independent of the direction of flow. Nield (1987*b*) pointed out, as he did for the porous layer (Nield 1987*a*), that assuming that the effect of the throughflow is invariably stabilizing is misleading, and proposed an explanation that the combination of different types of boundary condition may result in the throughflow having a destabilizing effect. The new features uncovered by Nield (1987*b*) are summarized as follows. First, the asymptotic relation $R^{\mathrm{c}} \sim \gamma^n$, where R^{c} is the critical Rayleigh number of the fluid layer, is found as γ becomes large, where γ is the throughflow strength and n is either 0, 1, 2, 3, or 4 depending on the boundary conditions imposed. Secondly, the destabilizing effects of the throughflow when the flow is from a dynamically rigid and thermally conducting boundary to a dynamically free and thermally insulating boundary may be due to three mechanisms. Third, when Pr is close to unity the amount of destabilization is small, but this is not true when Pr is either large or small. We will examine these features in detail in §§3 and 4.

In this study, we consider the throughflow effects on the buoyantly driven instability in superposed fluid and porous layers. The interface between the fluid and

porous layers is a rather unrestricted boundary in terms of momentum and heat transfer. On the interface, we impose continuity of vertical velocity, temperature, heat flux, and normal stress, and so on, although none of them is fixed. Accordingly, this interface boundary is much less restrictive both dynamically and thermally than either a rigid, or free, or conducting, or insulating boundary. Thus, according to Nield (1987*a*, *b*), the destabilizing effect of the throughflow may be enhanced in the combined-layers system because of the presence of a much less restrictive boundary. Another interesting point of the current study is the influence of Prandtl number on the throughflow effect. In the porous layer, the convective stability is independent of Pr_m, the Prandtl number of the porous layer, whereas in the fluid layer Pr has a considerable influence on the stability characteristics. In the superposed fluid and porous layer system with a rather unrestricted boundary in between, the Prandtl number may thus play a complicated role in determining the stability characteristics of the system.

Without considering throughflow, several investigators have investigated the problem of convective instability in superposed fluid and porous layers. Nield (1977) accounted for surface-tension effects at a deformable upper surface. Somerton & Catton (1982) included viscous effects on the boundary of the porous layer by including the Brinkman term in the Darcy equation. Chen & Chen (1988), using the Darcy equation in the porous layer and Beavers & Joseph's (1967) boundary condition on the interface between the fluid and porous layers, found that the depth ratio ζ plays a crucial role on the stability characteristics. Their theoretical results were later verified by their experiments (Chen & Chen 1989). Taslim & Narusawa (1989) studied the convective stability in both a fluid layer sandwiched between two porous layers and a porous layer sandwiched between two fluid layers. No publication, to the author's knowledge, has incorporated a throughflow effect into the superposed-layers problem.

For the present study, the depth ratio, Prandtl number, and the throughflow strength are the parameters which are considered to be influential. A wide-ranging parametric study is conducted so that an extensive discussion on throughflow effects on the convective stability of a superposed-layers system can be made. The critical Rayleigh number and associated wavenumber account for the stability characteristics. The eigenfunction of the perturbed vertical velocity and temperature and the corresponding streamline patterns and isotherms provide physical insight into the nature of the instability.

2. Problem formulation

We consider a porous layer of thickness d_m underlying a fluid layer of thickness d with throughflow of constant vertical velocity w_0. The layers are horizontal and of infinite extent in the horizontal direction. The top and bottom boundaries are dynamically rigid walls maintained at different constant temperatures, which are low at the top and high at the bottom. A Cartesian coordinate system is chosen with the origin at the interface between the porous and fluid layers and the z-axis vertically upward. The continuity, momentum, and energy equations for the fluid layer are, respectively,

$$\nabla \cdot \boldsymbol{u} = 0, \tag{1}$$

$$\rho_0 \left[\frac{\partial \boldsymbol{u}}{\partial t} + \boldsymbol{u} \cdot \nabla \boldsymbol{u}\right] = -\nabla P + \mu \nabla^2 \boldsymbol{u} - \rho_0 g[1 - \alpha(T - T_0)]\,\boldsymbol{k}, \tag{2}$$

$$\frac{\partial T}{\partial t}+\boldsymbol{u}\cdot\boldsymbol{\nabla}T=\kappa_{\mathrm{f}}\nabla^2 T. \tag{3}$$

The corresponding equations for the porous layer are (Somerton & Catton 1982)

$$\boldsymbol{\nabla}\cdot\boldsymbol{u}_{\mathrm{m}}=0, \tag{4}$$

$$\rho_0\left[\frac{1}{\phi}\frac{\partial \boldsymbol{u}_{\mathrm{m}}}{\partial t}+\frac{B}{K}|\boldsymbol{u}_{\mathrm{m}}|\boldsymbol{u}_{\mathrm{m}}\right]=-\frac{\mu}{K}\boldsymbol{u}_{\mathrm{m}}-\boldsymbol{\nabla}P_m-\rho_0 g[1-\alpha(T_{\mathrm{m}}-T_0)]\boldsymbol{k}, \tag{5}$$

$$G_{\mathrm{m}}\frac{\partial T_{\mathrm{m}}}{\partial t}+\boldsymbol{u}_{\mathrm{m}}\cdot\boldsymbol{\nabla}T_{\mathrm{m}}=\kappa_{\mathrm{m}}\nabla^2 T_{\mathrm{m}}. \tag{6}$$

In both sets of equations, the Boussinesq approximation has been applied and the thermal expansion coefficient α is defined as

$$\alpha=-\frac{1}{\rho_0}\left[\frac{\partial\rho}{\partial T}\right]_P. \tag{7}$$

The permeability of the porous medium is denoted by K. For a porous medium in which the solid phase consists of glass spheres, K is obtained from the Kozeny–Carmen relation (Combarnous & Bories 1975),

$$K=\frac{d_{\mathrm{g}}^2}{172.8}\frac{\phi^3}{(1-\phi)^2}. \tag{8}$$

in which d_{g} is the diameter of the spheres and ϕ the porosity.

In these equations, $\boldsymbol{u}$ denotes the velocity vector, P the pressure, T the temperature, and $\boldsymbol{k}$ the unit vector in the z-direction. The subscript m denotes the porous medium and f the fluid layer, and subscript 0 denotes a condition at the interface. μ is the dynamic viscosity, G_{m} the ratio of heat capacity of the two layers $(\rho_0 C_p)_{\mathrm{m}}/(\rho_0 C_p)_{\mathrm{f}}$, g is the gravitational acceleration, κ_{f} the thermal diffusivity of the fluid, and κ_{m} the thermal diffusivity of the porous medium, where $\kappa_{\mathrm{m}}=\phi\kappa_{\mathrm{f}}+(1-\phi)\kappa_{\mathrm{g}}$, κ_{g} being the thermal diffusivity of the solid part of the porous medium.

It is known that in a porous medium the inclusion of inertial effects by adding $\boldsymbol{u}_{\mathrm{m}}\cdot\boldsymbol{\nabla}\boldsymbol{u}_{\mathrm{m}}$ cannot be correct. Beck (1972) pointed out that this term vanishes identically if the flow is unidirectional and hence cannot represent the inertial effect (increase in drag) in that case. For many naturally occurring porous media, Nield & Joseph (1985) showed that $|\boldsymbol{u}_{\mathrm{m}}|\boldsymbol{u}_{\mathrm{m}}$ is the appropriate inertia term in the momentum equation, which implies that the effect of inertia is a drag term quadratic in the velocity $\boldsymbol{u}_{\mathrm{m}}$. The coefficient B, which is called the form drag constant, is independent of the viscosity and the other properties of the fluid, but is dependent on the geometry of the medium. It can be expressed as (Georgiadis & Catton 1986)

$$B=\frac{1.75d_{\mathrm{g}}}{150(1-\phi)}. \tag{9}$$

Experimental support for this form of the quadratic drag is described by Ward (1964), while the many experimental results summarized by MacDonald *et al.* (1979) are consistent with this form.

The boundary conditions are that at the upper boundary $T=T_{\mathrm{u}}$ and the horizontal velocity components vanish and the vertical velocity is w_0; at the lower boundary $T=T_{\mathrm{l}}$, and the vertical component of the velocity is w_0. At the interface the temperature, the normal component of the heat flux, and the normal stress are

continuous. Since in the Darcy equation there is no viscous stress, continuity of shear stress across the interface cannot be enforced. Thus, we use the condition proposed by Beavers & Joseph (1967) in which the slip in the tangential velocity is proportional to the vertical gradient of the tangential velocity in the fluid. In the horizontal directions we have periodic boundary conditions.

The basic state is steady and the velocity is w_0 in the vertical direction and zero in the horizontal directions:

$$\boldsymbol{u} = \boldsymbol{u}_{\mathrm{m}} = w_0 \boldsymbol{k}. \tag{10}$$

After applying the boundary conditions on the energy equations, we obtain the basic temperature distributions in the two layers:

$$T_{\mathrm{b}} = T_0 + \frac{T_0 - T_{\mathrm{u}}}{\mathrm{e}^{\gamma} - 1}(1 - \mathrm{e}^{(\gamma/d)z}), \quad 0 \leqslant z \leqslant d, \tag{11}$$

$$T_{\mathrm{mb}} = T_0 - \frac{T_{\mathrm{l}} - T_0}{\mathrm{e}^{-\gamma_{\mathrm{m}}} - 1}(1 - \mathrm{e}^{(\gamma_{\mathrm{m}}/d_{\mathrm{m}})z}), \quad -d_{\mathrm{m}} \leqslant z \leqslant 0, \tag{12}$$

where T_0 is the interface temperature, and $\gamma = w_0 d/\kappa_{\mathrm{f}}$ and $\gamma_{\mathrm{m}} = w_0 d_{\mathrm{m}}/\kappa_{\mathrm{m}}$ represent the throughflow strength, or the Péclet number, in the fluid and porous layers, respectively. The subscript b denotes the basic state.

The governing equations are linearized in the usual manner. For the momentum equations (2) and (5), we operate with $\boldsymbol{\nabla} \times \boldsymbol{\nabla} \times$ and then take the vertical component to eliminate the pressure. To render the equations non-dimensional, we choose separate lengthscales for the two layers so that both are of unit depth (Nield 1977). In this manner, the detailed flow fields in both the fluid and porous layers can be clearly discerned for all depth ratios ($\zeta = d/d_{\mathrm{m}}$). For the fluid layer, we choose the characteristic length as d, time as d^2/κ_{f}, velocity as κ_{f}/d, and temperature as $T_0 - T_{\mathrm{u}}$. For the porous layer, the corresponding characteristic quantities are d_{m}, $d_{\mathrm{m}}^2/\kappa_{\mathrm{m}}$, $\kappa_{\mathrm{m}}/d_{\mathrm{m}}$, and $T_{\mathrm{l}} - T_0$.

The non-dimensional equations, written in the same notation as their dimensional counterparts, are

$$\left[\frac{1}{Pr}\left(\frac{\partial}{\partial t} + \gamma\frac{\partial}{\partial z}\right) - \nabla^2\right]\nabla^2 W - R\nabla_2^2 T = 0, \tag{13}$$

$$\left[\frac{\partial}{\partial t} + \gamma\frac{\partial}{\partial z} - \nabla^2\right]T + W\frac{\gamma\,\mathrm{e}^{\gamma z}}{1 - \mathrm{e}^{\gamma}} = 0, \tag{14}$$

$$\left[\frac{\delta^2}{\phi Pr_{\mathrm{m}}}\left(\frac{\partial}{\partial t} + B_{\mathrm{m}}|\gamma_{\mathrm{m}}|\right) + 1\right]\nabla_{\mathrm{m}}^2 W_{\mathrm{m}} - R_{\mathrm{m}}\nabla_{2\mathrm{m}}^2 T_{\mathrm{m}} = 0, \tag{15}$$

$$\left[G_{\mathrm{m}}\frac{\partial}{\partial t} + \gamma_{\mathrm{m}}\frac{\partial}{\partial z_{\mathrm{m}}} - \nabla_{\mathrm{m}}^2\right]T_{\mathrm{m}} + W_{\mathrm{m}}\frac{-\gamma_{\mathrm{m}}\,\mathrm{e}^{\gamma_{\mathrm{m}} z_{\mathrm{m}}}}{1 - \mathrm{e}^{-\gamma_{\mathrm{m}}}} = 0. \tag{16}$$

All the variables are small perturbation quantities and $\nabla_2^2 = \partial^2/\partial x^2 + \partial^2/\partial y^2$ is the horizontal Laplacian, and ∇_{m} and $\nabla_{2\mathrm{m}}^2$ are the Laplacian and horizontal Laplacian of the porous medium. The quantity $B_{\mathrm{m}} = Bd_{\mathrm{m}}/K$ is a constant. The Rayleigh number for the fluid layer is

$$R = g\alpha(T_0 - T_{\mathrm{u}})\,d^3/(\nu\kappa_{\mathrm{f}}). \tag{17}$$

For the porous layer, the Rayleigh number is defined in terms of the permeability as

$$R_{\mathrm{m}} = g\alpha(T_{\mathrm{l}} - T_0)\,d_{\mathrm{m}} K/(\nu\kappa_{\mathrm{m}}) = R\zeta^{-4}(\delta\epsilon_T)^2, \tag{18}$$

where $\delta = K^{\frac{1}{2}}/d_{\mathrm{m}}$ is the Darcy number, ϵ_T the thermal diffusivity ratio $\kappa_{\mathrm{f}}/\kappa_{\mathrm{m}}$, $Pr = \nu/\kappa_{\mathrm{f}}$ and $Pr_{\mathrm{m}} = \nu/\kappa_{\mathrm{m}}$ the Prandtl numbers for the fluid and porous layers, respectively, and ν the kinematic viscosity of the fluid.

The dimensionless boundary conditions at the top and bottom walls are

$$\left.\begin{aligned} W = T = \frac{\partial W}{\partial z} = 0 \quad \text{at} \quad z = 1, \\ W_{\mathrm{m}} = T_{\mathrm{m}} = 0 \quad \text{at} \quad z_{\mathrm{m}} = -1, \end{aligned}\right\} \tag{19}$$

and those at the interface are

$$W = \frac{\zeta}{\epsilon_T} W_{\mathrm{m}}, \quad T = \frac{\epsilon_T}{\zeta} T_{\mathrm{m}}, \tag{20}$$

$$\frac{\partial T}{\partial z} = \frac{\partial T_{\mathrm{m}}}{\partial z_{\mathrm{m}}}, \tag{21}$$

$$\left(3\nabla_2^2 + \frac{\partial^2}{\partial z^2}\right)\frac{\partial W}{\partial z} - \frac{\gamma}{Pr}\frac{\partial^2 W}{\partial z^2} = -\frac{\zeta^4}{\epsilon_T}\left[\frac{1}{\delta^2} + \frac{B_{\mathrm{m}}|\gamma_{\mathrm{m}}|}{Pr_{\mathrm{m}}}\right]\frac{\partial W_{\mathrm{m}}}{\partial z_{\mathrm{m}}}. \tag{22}$$

In addition, the Beavers–Joseph boundary condition,

$$\frac{\partial^2 W}{\partial z^2} = \frac{\beta\zeta}{\delta}\frac{\partial W}{\partial z} - \frac{\beta\zeta^3}{\epsilon_T}\left[\frac{1}{\delta} + \frac{B_{\mathrm{m}}|\gamma_{\mathrm{m}}|\delta}{Pr_{\mathrm{m}}}\right]\frac{\partial W_{\mathrm{m}}}{\partial z_{\mathrm{m}}}, \tag{23}$$

is enforced at the interface, where the constant β ranges from 0.1 to 4 as determined experimentally by Beavers & Joseph (1967). From the experimental viewpoint, to reconcile the perturbation boundary condition $W = 0$ with the presence of a prescribed finite vertical throughflow, it is physically reasonable to expect that the upper and lower rigid boundaries have very low permeability such that the pressure drop across each boundary is sufficiently large to sustain the throughflow. This is a challenge in the experiment.

We perform a normal mode expansion of the dependent variables in both the fluid and porous layers as follows:

$$(W, T) = [\Omega(z), \Theta(z)] f(x, y)\, \mathrm{e}^{st}, \tag{24}$$

where

$$\nabla_2^2 f + a^2 f = 0,$$

and similarly for the variables in the porous layer. The growth factors s and s_{m} for both layers are generally complex. We use D and D_{m} to denote the differential operators $\mathrm{d}/\mathrm{d}z$ and $\mathrm{d}/\mathrm{d}z_{\mathrm{m}}$, respectively, and obtain an eigenvalue problem consisting of the following ordinary differential equations:

$$\left[\frac{1}{Pr}(s + \gamma\mathrm{D}) - (\mathrm{D}^2 - a^2)\right](\mathrm{D}^2 - a^2)\,\Omega = -a^2 R\Theta, \tag{25}$$

$$[s + \gamma\mathrm{D} - (\mathrm{D}^2 - a^2)]\,\Theta + \Omega\frac{\gamma\,\mathrm{e}^{\gamma z}}{1 - \mathrm{e}^{\gamma}} = 0, \tag{26}$$

$$\left[\frac{\delta^2}{\phi\, Pr_{\mathrm{m}}}(s_{\mathrm{m}} + B_{\mathrm{m}}|\gamma_{\mathrm{m}}|) + 1\right](\mathrm{D}_{\mathrm{m}}^2 - a_{\mathrm{m}}^2)\,\Omega_{\mathrm{m}} = -a_{\mathrm{m}}^2 R_{\mathrm{m}}\,\Theta_{\mathrm{m}}, \tag{27}$$

$$[G_{\mathrm{m}}\, s_{\mathrm{m}} + \gamma_{\mathrm{m}}\,\mathrm{D}_{\mathrm{m}} - (\mathrm{D}_{\mathrm{m}}^2 - a_{\mathrm{m}}^2)]\,\Theta_{\mathrm{m}} + \Omega_{\mathrm{m}}\frac{-\gamma_{\mathrm{m}}\,\mathrm{e}^{\gamma_{\mathrm{m}} z_{\mathrm{m}}}}{1 - \mathrm{e}^{-\gamma_{\mathrm{m}}}} = 0. \tag{28}$$

In these final equations, we have non-dimensional horizontal wavenumbers a and a_m, which are the separation constants of the normal mode expansion. Since the dimensional horizontal wavenumbers must be the same for the fluid and porous layers if matching of solutions in the two layers is to be possible, we must have $a/d = a_m/d_m$ and hence $\zeta = a/a_m$. The boundary conditions on the top and the bottom are

$$\Omega(1) = \Theta(1) = \mathrm{D}\Omega(1) = \Omega_m(-1) = \Theta_m(-1) = 0, \tag{29}$$

and those at the interface are

$$\Omega = \frac{\zeta}{\epsilon_T}\Omega_m, \quad \Theta = \frac{\epsilon_T}{\zeta}\Theta_m, \tag{30}$$

$$\mathrm{D}\Theta = \mathrm{D}\Theta_m, \tag{31}$$

$$\left[\mathrm{D}^3 - \frac{\gamma}{Pr}\mathrm{D}^2 - 3a^2\mathrm{D}\right]\Omega = -\frac{\zeta^4}{\epsilon_T}\left[\frac{1}{\delta^2} + \frac{B_m|\gamma_m|}{Pr_m}\right]\mathrm{D}_m\Omega_m, \tag{32}$$

$$\left[\mathrm{D}^2 - \frac{\beta\zeta}{\delta}\mathrm{D}\right]\Omega = -\frac{\beta\zeta^3}{\epsilon_T}\left[\frac{1}{\delta} + \frac{B_m|\gamma_m|\delta}{Pr_m}\right]\mathrm{D}_m\Omega_m. \tag{33}$$

The eigenvalue problem consists of a sixth-order ODE in the fluid layer and a fourth-order ODE in the porous layer, with ten boundary conditions.

From previous studies we know that the principle of exchange of instabilities holds for thermal convection with throughflow in both the fluid layer (Nield 1987*b*) and the porous layer (Homsy & Sherwood 1976; Jones & Persichetti 1986; Nield 1987*a*). We assume that the principle also holds for the present situation so that in the calculations s and s_m are set to be zero identically. We use a shooting method along with the so-called unit disturbance method to solve these ODEs with corresponding boundary conditions. For details of the computational procedure, the reader is referred to Chen, Chen & Pearlstein (1991).

3. Results

Since the parameter space of this problem is large, we summarize the parameters for convenience as follows: we have δ, B_m, β, ϵ_T, and ϕ as given, R_m^c (and R^c) is the eigenvalue to be solved with varying a_m (and a), Pr_m (and Pr), and γ_m (and γ). Note that R_m^c, a_m, Pr_m, and γ_m are related explicitly to R^c, a, Pr, and γ, respectively. The details of the values used are illustrated in the following. We assume that the porous medium consists of 3 mm diameter glass beads with random packing, which results in a porosity $\phi = 0.389$. According to (8) and (9), the permeability K and the form drag constant B are thus equal to 8.2123×10^{-5} cm^2 and 5.7283×10^{-3} cm, respectively, and thus $B_m = 209.25$. We also assume the depth of the porous layer to be $d_m = 3$ cm, giving a Darcy number $\delta = 3.02 \times 10^{-3}$. The Beavers–Joseph constant β is chosen to be 0.1 and the thermal diffusivity ratio ϵ_T is fixed to be 0.725 in the calculations.

Four different depth ratios $\zeta = 0.1$, 0.2, 0.5, and 1 are considered. The Prandtl number of the porous medium Pr_m, related to the Prandtl number of the fluid layer Pr by $Pr = Pr_m/\epsilon_T$, is considered to be either 0.1, 1, or 100. The Péclet number of the porous medium γ_m, related to γ of the fluid layer by $\gamma = \gamma_m\zeta/\epsilon_T$, varies from -10 to 10. The R_m^c (and R^c) and associated critical wavenumber a_m^c (and a^c) are used to

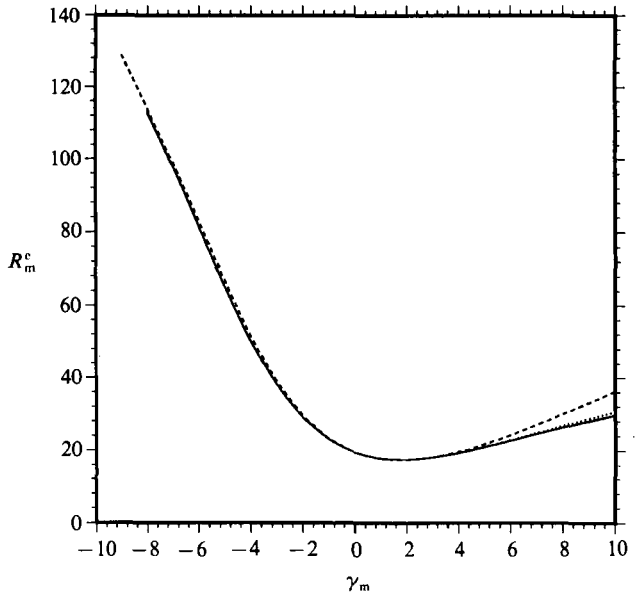

FIGURE 1. Variation of critical R_m with γ_m at $\zeta = 0.1$: ——, $Pr_m = 100$; · · · · ·, $Pr_m = 1$; – – – –, $Pr_m = 0.1$.

	Present		Homsy & Sherwood	
γ_m	a_m^c	R_m^c	a_m^c	R_m^c
0	3.14	39.4703	3.1	40
2	3.29	45.0682	3.3	45
4	3.79	61.6487	3.8	62
6	4.73	86.5861	4.7	86
8	6.09	114.7731	6.1	114
10	7.61	143.4251	7.6	143

TABLE 1. Comparison between the present results at $\zeta = 10^{-4}$ and those of Homsy & Sherwood (1976)

	Present		Chen & Chen	
ζ	a_m^c	R_m^c	a_m^c	R_m^c
0.1	2.15	19.5467	2.15	19.5718
0.2	13.01	3.3982	13.03	3.3979
0.5	5.46	0.00930	5.46	0.00928
1.0	2.79	0.006654	2.79	0.006651

TABLE 2. Comparison between the present results and those of Chen & Chen (1988, $\delta = 0.003012$, $\epsilon_T = 0.725$) for various ζ

measure the stability characteristics. The eigenfunctions of the perturbed vertical velocity Ω_m (and Ω) and temperature Θ_m (and Θ) serve to give physical insight into the nature of the instability.

3.1. *Verification of computer code*

Before we discuss the calculation for the superposed fluid and porous layers, the case of an approximately pure porous layer $\zeta = 10^{-4}$ is studied so that the results can be checked with the existing results of Homsy & Sherwood (1976) to verify the accuracy of the computer code to be used. Note that the momentum equation for the porous medium used in the current study and that in Homsy & Sherwood differ by the inertia term. After non-dimensionalizing, nevertheless, the inertia term becomes negligible as stated previously and thus the formulations of these two studies are essentially the same. The calculated results in terms of R_m^c and a_m^c for various γ_m are shown in table 1. One can see that the present results are in excellent agreement with those of Homsy & Sherwood (1976, figure 1).

Another computational check is possible for the case of $\gamma_m = 0$, considered by Chen & Chen (1988). Note that if $\gamma = 0$ and $\gamma_m = 0$ then both the denominator and numerator of the last term of (26) and (28) are, respectively, zero. Thus, use of L'Hôpital's rule on these terms is necessary. In table 2, one can see that the present results and those of Chen & Chen are in very good agreement.

3.2. *Depth ratio* $\zeta = 0.1$

For $\zeta = 0.1$, we consider three Prandtl numbers, $Pr_m = 0.1$, 1, and 100, and $-10 \leqslant \gamma_m \leqslant 10$. The positive γ_m accounts for the upward throughflow (hereafter we call it upflow) and the negative γ_m for the downward throughflow (downflow). One can see from figure 1, for all Pr_m values considered, that the downflow stabilizes the motionless state, and the upflow destabilizes it for $0 \leqslant \gamma_m \leqslant 1.8$ and stabilizes it for higher γ_m. The effect of downflow is much larger than that of upflow. The influence of Pr_m on R_m^c is insignificant. It is also found that the minimum critical a_m^c occurs at $\gamma_m = 0$; which means that at $\zeta = 0.1$ the throughflow always tends to reduce the critical wavelength. The effect of Pr_m on the critical a_m is also insignificant. Notice that the calculations stop at $\gamma_m = -7$ for $Pr_m = 100$, at $\gamma_m = -8$ for $Pr_m = 1$, and at $\gamma_m = -9$ for $Pr_m = 0.1$ because of divergence of the shooting iteration.

To gain physical insight into the onset of the convection, we illustrate the eigenfunctions of vertical velocity Ω and corresponding streamline patterns in figure 2. For each case presented, the value of Ω has been normalized so that its maximum magnitude is unity, and the width of the streamline plot is half the critical wavelength, which differs from case to case. In figure 2, $Pr_m = 1$ is considered and γ_m is chosen to be -8, -5, 0, 1.8, 5 and 10, of which $\gamma_m = 1.8$ is for the minimum R_m^c. For $\gamma_m = 0$ (see figure 2*c*), the case without throughflow, as indicated by Chen & Chen (1988), the onset of convection occurs in both fluid and porous layers and the lengthscale of a convection cell is the sum of the depths of the two layers. As the downflow increases in strength (increasing $-\gamma_m$), as shown in figure 2(*b* and *a*), the convection cell at onset gradually moves downwards and decreases in size simultaneously. Since the effective lengthscale of the onset of convection reduces as $-\gamma_m$ increases, the motionless state becomes more stable and thus the downflow is stabilizing. For the upflow, figure 2(*d*) shows that at the most unstable state ($\gamma_m = 1.8$) the maximum of Ω is much closer to the fluid layer than the cases when $\gamma_m \leqslant 0$. The presence of the fluid layer above the porous layer causes the motionless fluid to be less stable when $0 < \gamma_m < 1.8$ since more convection occurs in the less

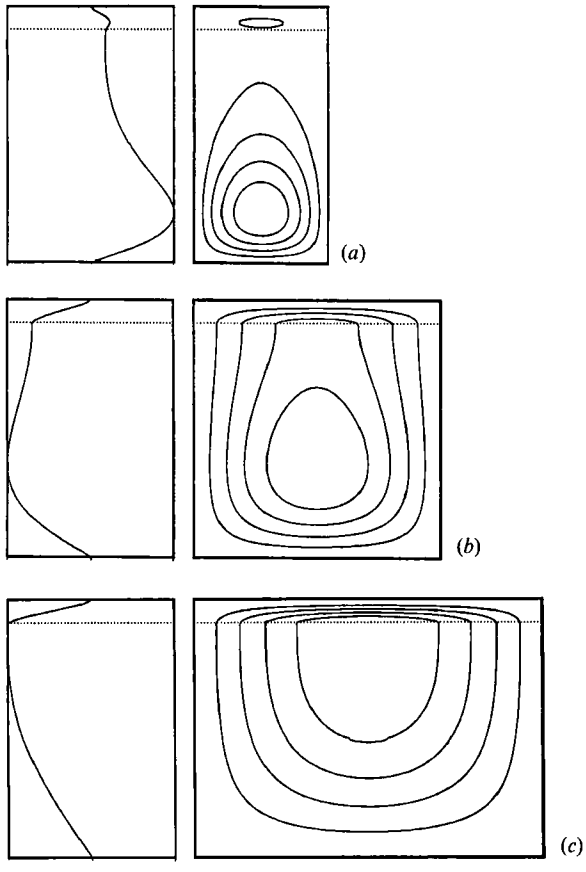

FIGURE 2(*a–c*). For caption see facing page.

restrictive fluid layer. However, as $\gamma_m > 1.8$, the upflow causes the onset of convection to occur more in the fluid layer with smaller effective lengthscale, which causes the flow to be more stable. Thus, the stabilizing effect due to the reduction of effective lengthscale overcomes the destabilization due to the occurrence of more convection in the fluid layer. Moreover, one can see from figure 1 that the downflow stabilizes the system more than the upflow does. That is because the downflow makes the onset occur in the more restrictive porous medium and the upflow makes it occur in the less restrictive fluid layer.

3.3. *Depth ratio* $\zeta = 0.2$

For $\zeta = 0.2$, from observations of the streamline patterns (not shown) we found the onset of convection to be largely confined to the fluid layer, which is similar to the findings of Chen & Chen (1988, figure 3*c*). There is very little variation among the streamline patterns for different γ_m. The critical a_m for $-10 \leqslant \gamma_m \leqslant 10$ are all larger than 13. We illustrate the variation of R_m^c with γ_m for three Pr_m values in figure 3. One can see that the R_m^c for $Pr_m = 1$ and 100 are very close while that for $Pr_m = 0.1$ is much larger. Similar results are also found for the variation of a_m^c with γ_m (not shown). In contrast to the case of $\zeta = 0.1$, the downflow destabilizes the system when $-1.5 \leqslant \gamma_m \leqslant 0$ and $-1.9 \leqslant \gamma_m \leqslant 0$ for $Pr_m = 1$ and 100, respectively. For $Pr_m = 0.1$, both downflow and upflow stabilize the motionless fluid. The upflow stabilizes

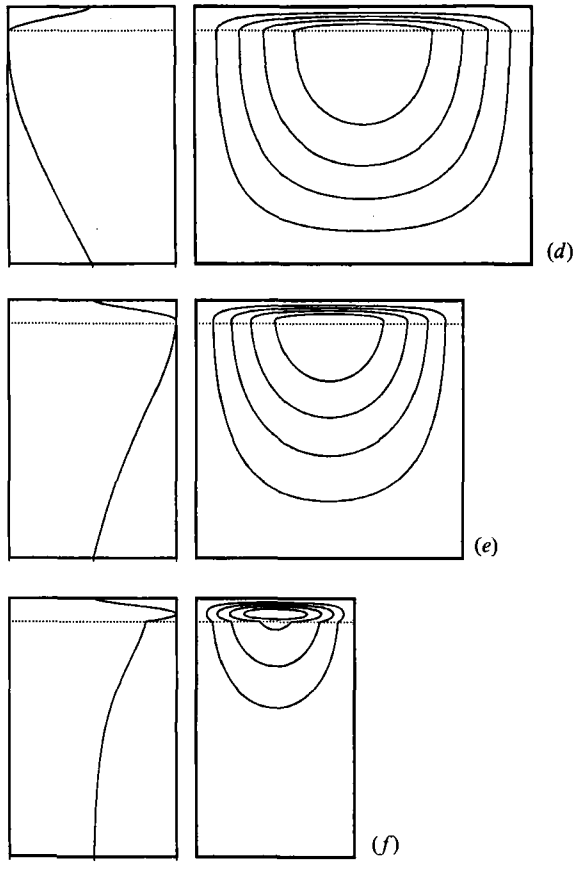

FIGURE 2. Streamline pattern (right) and Ω (and Ω_m) (left) for the onset of convection at $\zeta = 0.1$ and $Pr_m = 1$: (*a*) $\gamma_m = -8$, $a_m^c = 5.31$; (*b*) $\gamma_m = -5$, $a_m^c = 3.05$; (*c*) $\gamma_m = 0$, $a_m^c = 2.15$; (*d*) $\gamma_m = 1.8$, $a_m^c = 2.23$; (*e*) $\gamma_m = 5$, $a_m^c = 2.80$; (*f*) $\gamma_m = 10$, $a_m^c = 4.66$.

the system slightly more than the downflow does because the reduction of the scale of convection due to upflow is higher than that due to downflow.

3.4. *Depth ratio* $\zeta \geqslant 0.5$.

For $\zeta = 0.5$, we calculated the R_m^c and a_m^c for $-10 \leqslant \gamma_m \leqslant 4$ for $Pr_m = 0.1$ and $-10 \leqslant \gamma_m \leqslant 10$ for both $Pr_m = 1$ and 100. The results are shown in figure 4 for R_m^c. The calculation stops at $\gamma_m = 4$ for $Pr_m = 0.1$ because of divergence of the iteration. It is found that both the upflow and downflow stabilize the system for $Pr_m = 0.1$. For $Pr_m = 1$ and 100, the downflow is destabilizing when $-0.5 \leqslant \gamma_m \leqslant 0$ and is stabilizing for the other γ_m considered. As with $\zeta = 0.2$, the upflow stabilizes the system more than the downflow does although the difference is small. The destabilization due to throughflow for $Pr_m = 0.1$ is much larger than that for $Pr_m = 1$ and 100. The throughflow also reduces the critical wavelength of the convection cell because the minimum a_m^c occurs at $\gamma_m = 0$. The convection cell for $Pr_m = 0.1$ is generally smaller than those for $Pr_m = 1$ and 100.

The eigenfunctions of Ω and corresponding streamline patterns for five different γ_m for $Pr_m = 1$ are presented in figure 5. It is seen that the onset of convection is largely confined to the fluid layer, and in the porous layer heat is mainly transferred by conduction. As the downflow increases in strength, the onset of convection occurs

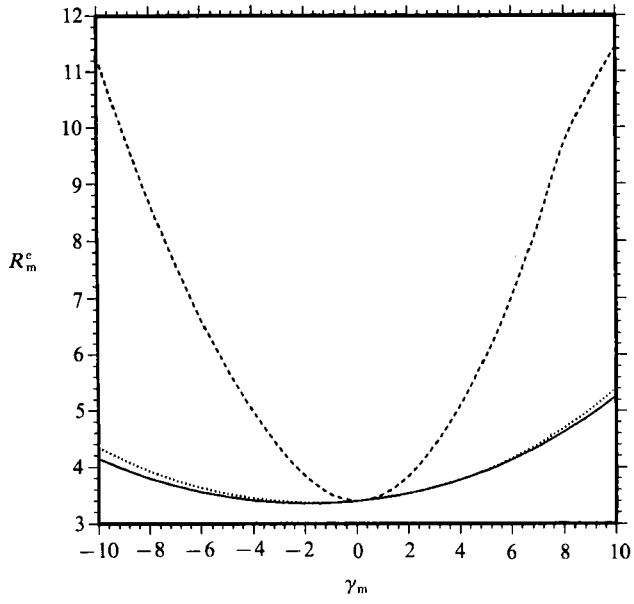

FIGURE 3. Variation of critical R_m with γ_m at $\zeta = 0.2$: ——, $Pr_m = 100$; · · · · ·, $Pr_m = 1$; – – – –, $Pr_m = 0.1$.

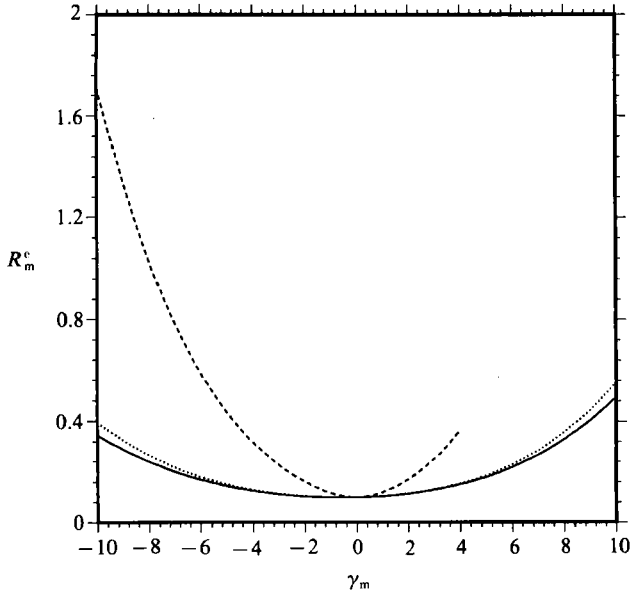

FIGURE 4. Variation of critical R_m with γ_m at $\zeta = 0.5$: ——, $Pr_m = 100$; · · · · ·, $Pr_m = 1$; – – – –, $Pr_m = 0.1$.

closer to the interface between the fluid and porous layers. As the upflow strength increases, the onset of convection appears to be shifting upwards to the top boundary. The reduction of the size of the convection cell is accompanied by an increase of the stability of the motionless state.

The results for $\zeta = 1$ of the variation of R_m^c with γ_m are shown in figure 6. The effect

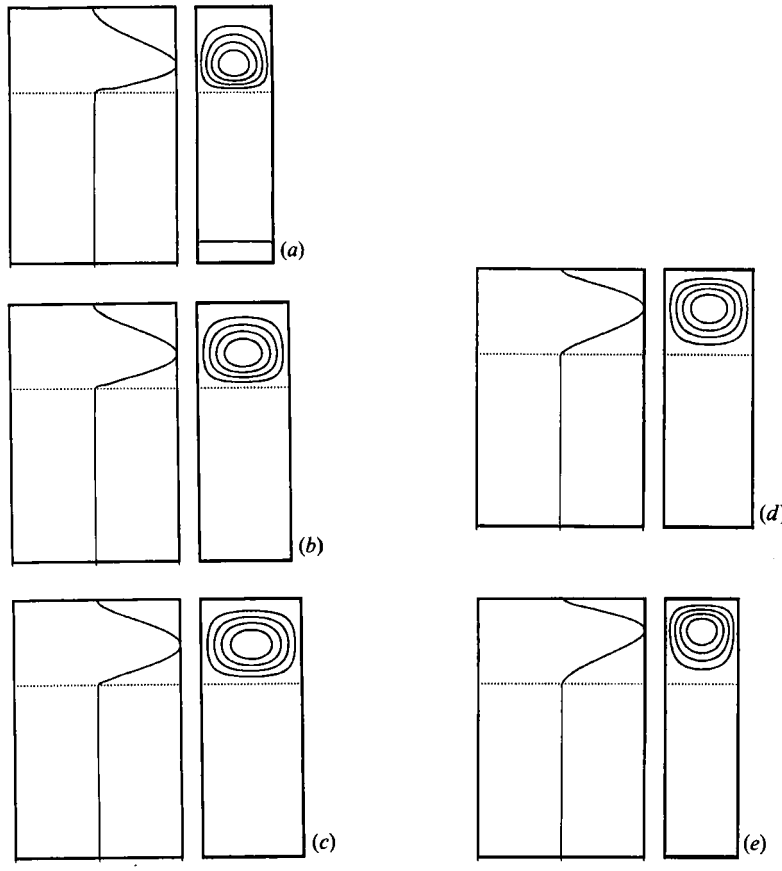

FIGURE 5. Streamline pattern (right) and Ω (and Ω_m) (left) for the onset of convection at $\zeta = 0.5$ and $Pr_m = 1$: (*a*) $\gamma_m = -10$, $a_m^c = 7.27$; (*b*) $\gamma_m = -5$, $a_m^c = 5.99$; (*c*) $\gamma_m = -0.5$, $a_m^c = 5.46$; (*d*) $\gamma_m = 5$, $a_m^c = 6.20$; (*e*) $\gamma_m = 10$, $a_m^c = 7.56$.

of throughflow on the stability characteristics for $\zeta = 1$ is similar to that for $\zeta = 0.5$. The throughflow stabilizes the system for $Pr_m = 0.1$. For $Pr_m = 1$ and 100, the throughflow again stabilizes the system except in the range of $-0.2 \leqslant \gamma_m \leqslant 0$ in which the downflow is destabilizing. The streamline patterns (not shown) illustrate similar phenomena to those of figure 5 while the shift of the convection cell at onset is enhanced due to the larger depth of the fluid layer. The reduction of effective lengthscale due to throughflow (except in the range of $-0.2 \leqslant \gamma_m \leqslant 0$) leads to a more stable motionless state.

4. Discussion

Nield (1987*a*, *b*) explained the destabilization by throughflow as the result of the combination of three different mechanisms. They are: first, the distortion of the basic-state temperature distribution which leads to the occurrence of maxima of Ω close to the position of the maxima of Θ; secondly, the momentum transport, which opposes the stabilizing effect of viscous diffusion when the throughflow is from a rigid to a free boundary; and thirdly, the thermal energy transport, which opposes the stabilizing effect of thermal diffusion when the throughflow is directed to an insulating boundary from a conducting boundary. The above conclusions apply to

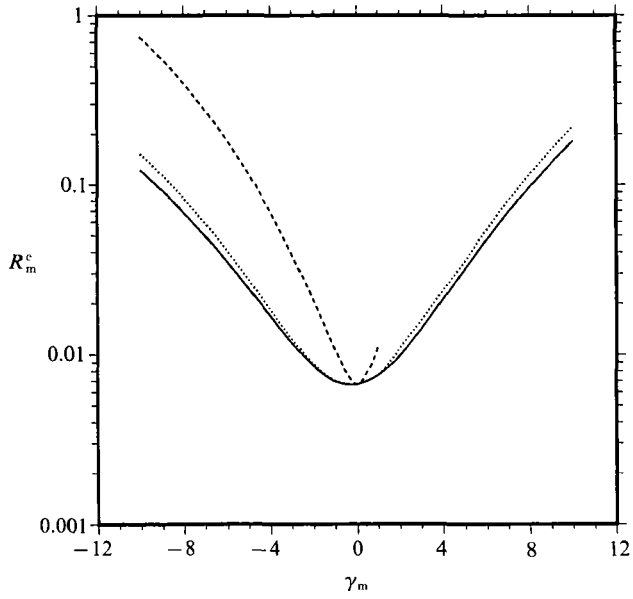

FIGURE 6. Variation of critical R_m with γ_m at $\zeta = 1$: ——, $Pr_m = 100$; · · · · ·, $Pr_m = 1$; – – – –, $Pr_m = 0.1$.

both fluid and porous layers. He also pointed out that in a fluid layer the destabilizing effect of throughflow is smaller when Pr is close to unity, but can be significant when Pr is either smaller or larger than unity. Regarding the asymptotic relation between the R^c and the throughflow strength γ, Nield (1987*b*) proposed that $R^c \sim \gamma^n$, in which n is either 0, 1, 2, 3, or 4 depending on the boundary conditions imposed. In the following, we focus on these statements and discuss them in relation to the results obtained in this study.

4.1. *Asymptotic relation* $R^c \sim \gamma^n$

Gershuni & Zhukhovitskii (1976, p. 236) addressed the situation wherein a fluid layer R^c increases with the throughflow strength γ according to $R^c \sim \gamma^3$. Nield (1987*b*) later presented a more comprehensive discussion in which $R^c \sim \gamma^3$ holds only for the case with two rigid boundaries. The relation becomes $R^c \sim \gamma$ for two free insulating boundaries, $R^c \sim \gamma^3$ for two rigid insulating boundaries or two free conducting boundaries and $R^c \sim \gamma^4$ when the throughflow is from a rigid insulating boundary and toward a rigid conducting boundary. In a porous layer, as γ_m becomes large, Nield (1987*a*) stated that the relation $R_m^c \sim \gamma_m^0$ holds for two free insulating boundaries, and $R_m^c \sim |\gamma_m|$ both for two rigid insulating boundaries and for one rigid insulating and one free insulating boundary when the throughflow is away from the latter.

In the present situation, the combination of a fluid and a porous layer makes the relation between the critical Rayleigh number and the throughflow strength different from a case involving just a single layer. For $\zeta = 0.1$, from figure 1 one can see that as $|\gamma_m|$ becomes large R_m^c increases with $|\gamma_m|$ according to the linear relation $R_m^c \sim |\gamma_m|$. In this case, the porous layer dominates the system by convection so that the effective layer thickness is proportional to $d_m/|\gamma_m|$. Therefore the relation $R_m^c \sim |\gamma_m|$ holds according to the definition of R_m in (18). We compared the slope of the curve

$\zeta \backslash Pr_m$	0.1	1	100
0.1	−0.1082	−0.1037	−0.1028
0.2	0	−0.00837	−0.01192
0.5	0	−0.00587	−0.00704
1.0	0	−0.00415	−0.00457

TABLE 3. The destabilizing factor in terms of $(R_m^c - R_{m0}^c)/R_{m0}^c$, in which R_{m0}^c is the R_m^c without throughflow, for various Pr_m and ζ

in figure 1 with that of Homsy & Sherwood (1976, figure 1) and found that the presence of a shallow fluid layer above the porous layer considerably influences the stabilizing effect due to throughflow in the porous layer. It is found that the downflow enhances the stabilizing effect and upflow reduces it. This is because the downflow ensures that the onset of convection is confined mostly to the more restrictive porous layer while the upflow causes the onset of convection to occur more in the less restrictive fluid layer.

For the case of $\zeta \geqslant 0.2$, the relation between R_m^c and γ_m is nonlinear as γ_m becomes large. For $\zeta = 0.2$, figure 3, the relation $R_m^c \sim \gamma_m^2$ holds for most cases except $Pr_m = 0.1$ with large positive γ_m in which $R_m^c \sim \gamma_m^3$ holds. For $\zeta = 0.5$ and 1, figures 4 and 6, respectively, the results support the relation $R_m^c \sim \gamma_m^2$ for all the cases considered. The results for $Pr_m = 0.1$ when γ_m is large positive are not available owing to the divergence of iteration.

4.2. *Prandtl-number effect*

The stability characteristics due to throughflow are independent of Pr_m in the porous layer but are dependent on Pr in the fluid layer. In the fluid layer, the results of Gershuni & Zhukhovitskii (1976, figure 106) show that with two rigid conducting boundaries R^c increases with decreasing Pr and the difference, in terms of the R^c and a^c, between $Pr = 0.1$ and 1 is larger than that between $Pr = 1$ and 10. Regarding the destabilization when the throughflow is away from a rigid boundary and toward a free boundary, the conclusion of Nield (1987*b*) indicates that the destabilizing effect of throughflow reaches a minimum for $Pr = 1$ and is larger for other Pr. In the combined fluid and porous layer system with rigid conducting boundaries at top and bottom and a rather unrestricted interface in between, we found that the influence of Pr_m (and Pr) becomes complex owing to the competition between the fluid and porous layers. In the case of $\zeta = 0.1$, the critical R_m^c values for $Pr_m = 0.1$, 1, and 100 are little different so that the Pr_m effect is negligible. By observing the streamline patterns for $Pr_m = 0.1$ (not shown) and comparing those with the corresponding ones for $Pr_m = 1$ in figure 2, we do not find significant differences between them. As for the destabilizing effect, we summarize the destabilizing factor in terms of $(R_m^c - R_{m0}^c)/R_{m0}^c$, in which R_{m0}^c is the R_m^c without throughflow, for various Pr_m and ζ in table 3. For $\zeta = 0.1$, the destabilizing factor decreases with increasing Pr_m. It is noted that the destabilizing factor for $\zeta = 0.1$ is generally much higher than that for a pure porous layer $\zeta = 0$ (Jones & Persichetti 1986, figure 1).

For $\zeta \geqslant 0.2$, the throughflow stabilizes the system much more for $Pr_m = 0.1$ than for $Pr_m = 1$ and 100; see figures 3, 4 and 6. This is consistent with the results for a pure fluid layer (Gershuni & Zhukhovitskii 1976, figure 106) because for $\zeta \geqslant 0.2$ the fluid layer dominates the system by convection. The destabilizing factor of throughflow, see table 3, is zero for $Pr_m = 0.1$ and decreases with increasing ζ but increases with Pr_m for $Pr_m = 1$ and 100. This is different from the pure fluid-layer

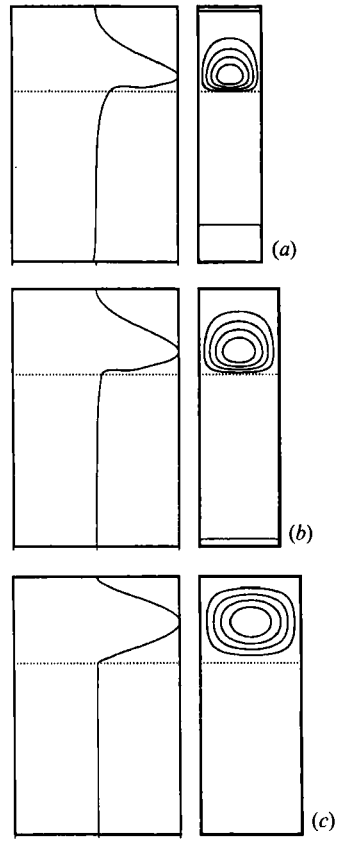

FIGURE 7. Streamline pattern (right) and Ω (and Ω_m) (left) for the onset of convection at $\zeta = 0.5$ and $Pr_m = 0.1$: (a) $\gamma_m = -10$, $a_m^c = 8.69$; (b) $\gamma_m = -5$, $a_m^c = 6.88$; (c) $\gamma_m = -0.5$, $a_m^c = 5.46$.

	$Pr_m = 0.1$			$Pr_m = 1$			$Pr_m = 100$		
ζ	γ_m	a_m^c	R_m^c	γ_m	a_m^c	R_m^c	γ_m	a_m^c	R_m^c
0.1	1.8	2.20	17.4307	1.8	2.23	17.5199	1.8	2.24	17.5376
0.2	0	13.0	3.3978	−1.5	13.0	3.3698	−1.9	13.0	3.3578
0.5	0	5.46	0.09928	−0.5	5.46	0.09872	−0.5	5.45	0.09860
1.0	0	2.79	0.006654	−0.2	2.79	0.006626	−0.2	2.79	0.006623

TABLE 4. The γ_m for minimum R_m^c and associated a_m^c for various ζ and Pr_m

case (Nield 1987*b*) in which the destabilizing factor is a minimum for $Pr = 1$. The existence of an underlying porous layer changes the destabilizing effect of the fluid layer owing to the variation of the Prandtl number. To gain some physical insight into the Prandtl-number effect, we present in figure 7 the streamline patterns for $\zeta = 0.5$ and $Pr_m = 0.1$ to compare with the corresponding case of $Pr_m = 1$ shown in figure 5. It is found that for smaller Pr_m the onset of the convection cell is closer to the interface and with smaller effective lengthscale. The reduction of lengthscale causes the motionless fluid for $\zeta = 0.5$ to be more stable for smaller Pr_m.

Note that, owing to the smallness of the Darcy number δ chosen in this study, the insensitivity of the stability characteristics to Pr_m in a porous medium may be

inferred from the scaled version of (15), in which the value of $\delta^2/(\phi Pr_m)$ is very small. Nevertheless, if the quantity $\delta^2/(\phi Pr_m)$ is of order of unity, Pr_m may play a significant role in determining the stability criteria. One, accordingly, might expect that $\delta^2/(\phi Pr_m)$ is a controlling parameter, rather than Pr_m itself, in a system such as a liquid metal in a very porous material where $\delta^2/(\phi Pr_m)$ may not be small.

4.3. *Destabilizing mechanisms*

For $\zeta \leqslant 0.1$, the upflow is destabilizing for $0 \leqslant \gamma_m \leqslant 1.8$. In the superposed-layers system, the upflow in the porous layer is away from a rigid conducting boundary to a boundary (the interface) on which both thermal and dynamical conditions are free. Therefore, according to Nield (1987*a*, *b*), the upflow destabilizes the porous layer, which implies that it destabilizes the system because the porous layer for $\zeta = 0.1$ dominates the system by convection. According to Jones & Persichetti (1986, figure 1), the throughflow away from a rigid conducting boundary to a free conducting boundary destabilizes the fluid in a porous layer when $0 \leqslant \gamma_m \leqslant 1$ with the destabilizing factor (defined in §4.2) being smaller than 0.04 (which is roughly estimated from figure 1 of Jones & Persichetti 1986). In the present situation of $\zeta = 0.1$, the destabilizing factor is more than 0.1 in a larger range, $0 \leqslant \gamma_m \leqslant 1.8$. This means that the presence of a shallow overlying fluid layer, enhances the destabilizing factor of the porous layer due to upflow by more than 2.5 times that of the pure porous-layer case and the range of destabilizing γ_m is almost doubled.

For $\zeta \geqslant 0.2$, the fluid layer dominates the system by convection and the downflow is destabilizing in some ranges of γ_m for $Pr_m = 1$ and 100. The range of destabilizing γ_m decreases with increasing ζ (see table 4). The downflow in the fluid layer is away from a rigid conducting boundary towards a thermally and dynamically free boundary and therefore destabilizes the fluid of the system. According to table 3, the destabilizing factor increases with Pr_m and decreases with increasing ζ. On comparing table 3 of the present study to table 1 of Nield (1987*b*, the case of $\zeta = \infty$), we found that the presence of an underlying porous layer enhances the destabilizing factor in the fluid layer for $Pr_m = 1$ and reduces it for $Pr_m = 0.1$ and 100.

From the discussion above, we can conclude that the second destabilizing mechanism proposed by Nield (1987*a*, *b*) also holds here from the viewpoint of the whole system. However, from the viewpoint of the fluid layer for $\zeta = 0.1$, the upflow, which is away from a free boundary towards a rigid boundary, destabilizes the fluid in the range $0 \leqslant \gamma_m \leqslant 1.8$. A similar statement can be made for the porous layer with $\zeta \geqslant 0.2$ for some range of γ_m depending on ζ and Pr_m. Accordingly, in the combined fluid and porous layer system, one can either stabilize or destabilize the motionless state in a particular layer by changing ζ or the direction and the strength of the throughflow or both. More precise control of stabilization or destabilization due to throughflow can possibly be obtained because both the stabilizing factor and destabilizing factor can be enhanced by a relatively large amount compared with those of each single layer. This discussion can also be applied to Nield's third destabilizing mechanism, thermal energy transfer from a thermally rigid boundary to a free boundary.

We now examine Nield's first destabilizing mechanism, which states that the distortion of the basic-state temperature distribution leads to the occurrence of the maximum of Ω close to the location of the maximum of Θ when the destabilization occurs. To examine this statement, we present the eigenfunction of Θ and corresponding isotherms for various ζ for $Pr_m = 1$. For $\zeta = 0.1$, the eigenfunction of Θ and corresponding isotherms are shown in figure 8. Comparing the maxima of Θ

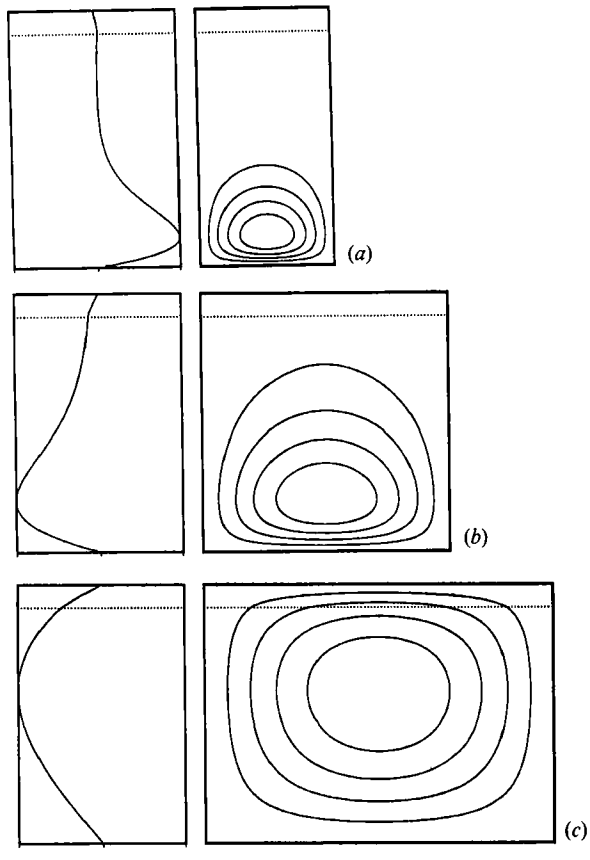

FIGURE 8(a–c). For caption see facing page.

with those of Ω in figure 2, we found that the distance between the maxima of Θ and Ω increases as the downflow strength decreases from $\gamma_m = -8$ to 0, where their separation is the largest. As the upflow strength increases from $\gamma_m = 0$ to 10, the separation decreases. The smallest distance does not occur at $\gamma_m = 1.8$, where the maximum destabilization occurs. Nield's first destabilizing mechanism does not apply for $\zeta = 0.1$ because the onset of convection occurs in both fluid and porous layers and the presence of the interface between the two layers makes the stability characteristics more complex than a single fluid or porous layer.

However, for $\zeta \geqslant 0.2$, the maximum of Θ does move closer to the maximum of Ω when the destabilizing effect dominates. We present the eigenfunction of Θ and corresponding isotherms for $\zeta = 0.5$ in figure 9 to compare with the corresponding Ω in figure 5. It is found that the distance between the maxima of Ω and Θ is smallest at $\gamma_m = -0.5$, when the system is in the most unstable state. Similar results are found in the case of $\zeta = 1$ where the vertical separation of the maxima of Ω and Θ is smallest at approximately $\gamma_m = -0.2$, when the system is most unstable.

5. Summary

From the above analyses, we found that the stability characteristics of superposed fluid and porous layers depend crucially on both the depth ratio ζ and the throughflow direction. For $\zeta = 0.1$, the upflow destabilizes the system when

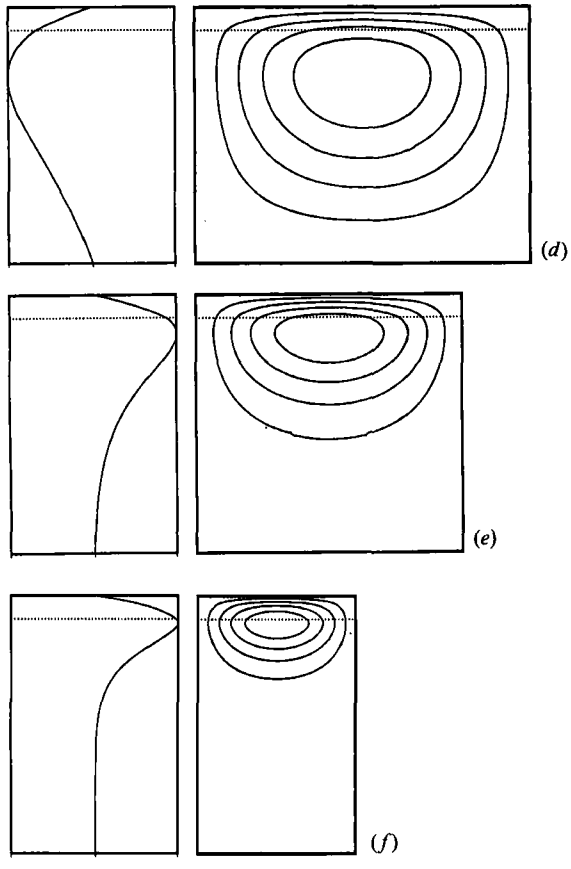

FIGURE 8. Isotherms (right) and Θ (and Θ_m) (left) for the onset of convection at $\zeta = 0.1$ and $Pr_m = 1$: (*a*) $\gamma_m = -8$; (*b*) $\gamma_m = -5$; (*c*) $\gamma_m = 0$; (*d*) $\gamma_m = 1.8$; (*e*) $\gamma_m = 5$; (*f*) $\gamma_m = 10$.

$0 \leqslant \gamma_m \leqslant 1.8$ and stabilizes it otherwise. The downflow stabilizes the system more than the upflow because the downflow causes the onset of convection to be confined largely to the largely restrictive porous layer while the upflow makes the onset of convection occur more in the less restrictive fluid layer. For $\zeta \geqslant 0.2$, the downflow destabilizes the system and the range of destabilizing γ_m varies with ζ and Pr_m. The stabilizing factor of upflow is about the same as that of downflow and both decrease with increasing Pr_m, consistent with the results obtained by Gershuni & Zhukhovitskii (1976) for the fluid layer.

We also discussed the relation between R_m^c and γ_m as $|\gamma_m|$ becomes large. For $\zeta = 0.1$, the relation is linear, $R_m^c \sim |\gamma_m|$. For $\zeta \geqslant 0.2$, the relation is second order, $R_m^c \sim \gamma_m^2$, although there is an exception for $Pr_m = 0.1$ at large positive γ_m where the relation $R_m^c \sim \gamma_m^3$ holds.

Regarding the destabilizing mechanism, the first and second mechanisms proposed by Nield (1987*a*, *b*) are confirmed by our results if considered from the viewpoint of the whole system. The third destabilizing mechanism is found to be valid for the case of $\zeta \geqslant 0.2$ in which the convection is largely confined to the fluid layer but does not apply for $\zeta = 0.1$ because the onset of convection occurs in both the fluid and porous layers. In applications, the configuration discussed here may provide more precise control of the buoyantly driven instability naturally arising in either a porous medium or a fluid layer by changing ζ or the strength and direction of throughflow

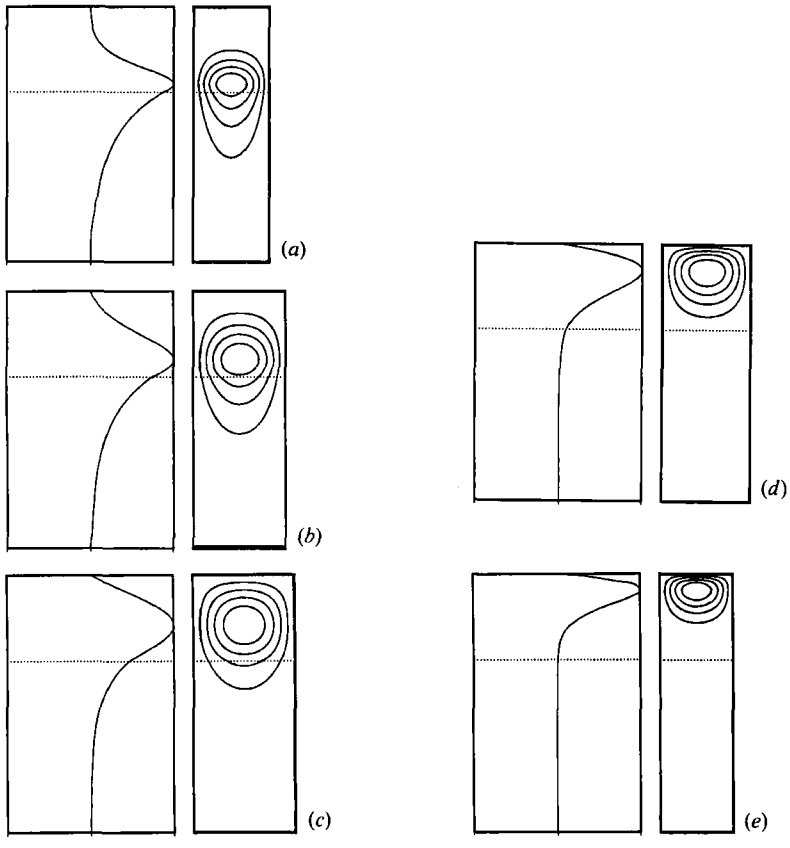

FIGURE 9. Isotherms (right) and Θ (and Θ_m) (left) for the onset of convection at $\zeta = 0.5$ and $Pr_m = 1$: (a) $\gamma_m = -10$; (b) $\gamma_m = -5$; (c) $\gamma_m = 0.5$; (d) $\gamma_m = 5$; (e) $\gamma_m = 10$.

or both because both the stabilizing and destabilizing factors can be enhanced more for a combined-layers systems than for a single-layer system and the range of destabilizing γ_m can be enlarged.

The correction of the English of the manuscript by one of the referees is gratefully acknowledged.

REFERENCES

BEAVERS, G. S. & JOSEPH, D. D. 1967 Boundary conditions at a naturally permeable wall. *J. Fluid Mech.* **30**, 197–207.

BECK, J. L. 1972 Convection in a box of porous material saturated with fluid. *Phys. Fluids* **15**, 1377–1383.

CHEN, F. & CHEN, C. F. 1988 Onset of finger convection in a horizontal porous layer underlying a fluid layer. *Trans. ASME* C: *J. Heat Transfer* **110**, 403–409.

CHEN, F. & CHEN, C. F. 1989 Experimental investigation of convective instability in a superposed fluid and porous layer when heated from below. *J. Fluid Mech.* **207**, 311–321.

CHEN, F., CHEN, C. F. & PEARLSTEIN, A. J. 1991 Convective instability in superposed fluid and anisotropic porous layers. *Phys. Fluids* A **3**, 556–565.

COMBARNOUS, M. A. & BORIES, S. A. 1975 Hydrothermal convection in saturated porous media. *Adv. Hydrosc.* **10**, 231–307.

GEORGIADIS, J. G. & CATTON, I. 1986 Prandtl number effect on Benard convection in porous media. *Trans. ASME* C: *J. Heat Transfer* **108**, 284–290.

GERSHUNI, G. Z. & ZHUKHOVITSKII, E. M. 1976 *Convective Stability of Incompressible Fluids*, pp. 235–240. Israel Program for Scientific Translations.

HOMSY, G. M. & SHERWOOD, A. E. 1976 Convective instabilities in porous media with through flow. *AIChE J.* **22**, 168–174.

JONES, M. C. & PERSICHETTI, J. M. 1986 Convective instability in packed beds with throughflow. *AIChE J.* **32**, 1555–1557.

KRISHNAMURTI, R. 1975 On cellular cloud patterns, Part 1: mathematical model. *J. Atmos. Sci.* **32**, 1353–1363.

MACDONALD, I. F., EL-SAYED, M. S., MOW, K. & DULLIEN, F. A. L. 1979 Flow through porous media – the Ergun equation revisited. *Indust. Engng Chem. Fundam.* **18**, 199–208.

NIELD, D. A. 1977 Onset of convection in a fluid layer overlying a layer of a porous medium. *J. Fluid Mech.* **81**, 513–522.

NIELD, D. A. 1987*a* Convective instability in porous media with throughflow. *AIChE J.* **33**, 1222–1224.

NIELD, D. A. 1987*b* Throughflow effects in the Rayleigh–Bénard convective instability problem. *J. Fluid Mech.* **185**, 353–360.

NIELD, D. A. & JOSEPH, D. D. 1985 Effect of quadratic drag on convection in a saturated porous medium. *Phys. Fluids* **28**, 995–997.

SHVARTSBLAT, D. L. 1968 The spectrum of perturbations and convective instability of a plane horizontal fluid layer with permeable boundaries. *Appl. Math. Mech.* (*PMM*) **32** , 266–271. (Transl. from *Prikl. Mat. Mekh.*)

SHVARTSBLAT, D. L. 1969 Steady convective motions in a plane horizontal fluid layer with permeable boundaries. *Fluid Dyn.* **4**, 54–59. (Transl. from *Izv. Akad. Nauk SSSR, Fiz. Zhid. i Gaza.*)

SHVARTSBLAT, D. L. 1971 Chislennoe issledovanie statsionarnogo konvektivnoge dvizheniya v ploskon gorizontal'nom, sloe zhidkosti. *Uchen. Zap. Perm Univ.* No. 248; *Gidrodinamika* **3**, 97.

SOMERTON, C. W. & CATTON, I. 1982 On the thermal instability of superposed porous and fluid layers. *Trans. ASME* C: *J. Heat Transfer* **104**, 160–165.

SOMERVILLE, R. C. J. & GAL-CHEN, T. 1979 Numerical simulation of convection with mean vertical motion. *J. Atmos. Sci.* **36**, 805–815.

SUTTON, F. M. 1970 Onset of convection in a porous channel with net through flow. *Phys. Fluids* **13**, 1931–1934.

TASLIM, M. E. & NARUSAWA, U. 1989 Thermal stability of horizontal superposed porous and fluid layers. *Trans. ASME* C: *J. Heat Transfer* **111**, 357–362.

WARD, J. C. 1964 Turbulent flow in porous media. *J. Hydraul. Div. ASCE* **90**, 1–13.

WOODING, R. A. 1960 Rayleigh instability of a thermal boundary layer in flow through a porous medium. *J. Fluid Mech.* **9**, 183–192.